Acta Mechanica Solida Sinica, Vol. 22, No. 6, December, 2009 ISSN 0894-9166
Published by AMSS Press, Wuhan, China.

CONCAVE BIOLOGICAL SURFACES FOR STRONG WET ADHESION**

Yewang Su[1] **Baohua Ji**[2*] **Yonggang Huang**[3*] **Kehchih Hwang**[1]

([1] *Department of Engineering Mechanics, Tsinghua University, Beijing* 100084, *China*)
([2] *Department of Applied Mechanics, Beijing Institute of Technology, Beijing* 100081, *China*)
([3] *Department of Civil and Environmental Engineering, Northwestern University, Evanston, IL* 60208, *USA*)

Received 1 July 2009, revision received 20 November 2009

ABSTRACT Plant leaves, insects and geckos are masters of adhesion or anti-adhesion by smartly designed refined surface structures with micro- and nano- 'technologies'. Understanding the basic principles in the design of the unique surface structures is of great importance in the manufacture or synthesis of micro- and nano- devices in MEMS or NEMS. This study is right inspired by this effort, focusing on the mechanics of wet adhesion between fibers having concave tips and a flat substrate via capillary forces. We show that the concave surface can effectively enhance the wet adhesion by reducing the effective contact angle of the fiber, firmly pinning the liquid bridge at its circumferential edge. A critical contact angle is identified below which the adhesion strength can achieve its maximum, being insensitive to the contact angle between the fiber and liquid. The analytical expression for the critical angle is derived. Then a tentative design for the profile of concave surfaces is proposed, considering the effects of chamfering size, deformation and buckling, etc. The effect of liquid volume on the wet adhesion of multiple-fiber system is also discussed.

KEY WORDS biological surface, wet adhesion, contact shape, concave surface, robustness, adhesion force

I. INTRODUCTION

Biological surfaces (plant leaves, gecko and insect attachment pads, etc.) have remarkable properties due to their unique surface structures that affect their adhesion and wetting properties. Leaves of many plants, which grow in extremely wet or extremely dry conditions, have developed the ability to repel or collect water. Several creatures, including insects, spiders and lizards/geckos, have a unique ability to cling to and detach from walls using their attachment systems. A pond skater (Gerris remigis) has the ability to walk upon a water surface without getting wet. Even the impact of rain droplets with a size greater than the strider does not make it immerse into water. The concepts and principles found in the living nature will be critically important to the design of novel engineering systems.

The study of animal wet adhesion, for many years a relatively neglected research area, has recently undergone a resurgence of intense interest. This is partly because of the promise of practical applications arising from the research — animal adhesive devices have many properties that are the envy of materials scientists, and partly because the application of recent advances in nano- and bio- technologies has produced a quantum leap forward in our understanding of these inspiring systems[1–3]. In contrast to

* Corresponding author. E-mail: bhji@bit.edu.cn (Baohua Ji); y-huang@northwestern.edu (Yonggang Huang)

** Project supported by the National Natural Science Foundation of China through Grant Nos. 10628205, 10732050 and 10872115, and National Basic Research Program of China through Grant No. 2007CB936803, and SRF-SEM for ROCS.

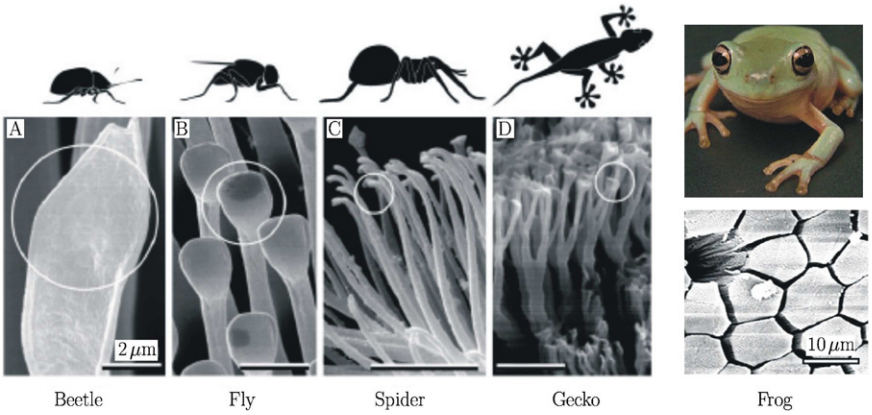

Fig. 1. The biological surfaces and their nano- and micro- surface structures.

the dry adhesion via van der Waals (vdW) forces, the 'wet adhesion' uses the capillary force via liquid bridge between the biological surfaces and the substrate, which has been widely adopted by many insects and animals from beetle, fly, spider, to gecko/lizard and tree frog. All of these insects and animals have powerful attachment systems covered by fine surface structures, such as setae or hair, as shown Fig.1. The roles of the surface structures including their size, geometry and hierarchy, have attracted intense research recently.

There are debates on the roles of the vdW force and capillary force on the biological adhesion and which plays the main role. Recent studies showed that these two mechanisms may both be crucial to the biological adhesion, and insects and animals may use both of them for strong and secure adhesion. A number of experimental measures[4–7] on the attachment devices, such as those of flies, spiders and geckos, and theoretical analyses[8–10], proved that biological systems indeed can use vdW forces to achieve strong adhesion with finely designed structures on the attachment systems. With the spirits of fracture mechanics[11–17], Gao and coworkers studied the effect of contact shapes on dry adhesion[18], and proposed an optimum shape of surface structure. They showed that the adhesive force can be enlarged by the reduction of the size of surface structures[10, 14, 19], and the adhesion strength becomes insensitive to existing flaws[15] and the contact shape[20] at nanometer-scales.

On the other hand, Huber et al.[21] provided the evidence for the contributions of capillary forces to the adhesion of geckos through nanomechanical measurements of wet adhesion of a single spatula. Furthermore, Sun et al.[22] found that the presence of water strongly affects the adhesion of geckos by measuring the adhesion force via continuously changing the relative humidities. These evidences show that gecko can use both the vdW force and the capillary force for their adhesion. In comparison with the vdW force the capillary force is a long range force, and can take effect at larger scales. The capillary force between a hemisphere and a plane was first studied by Orr several decades ago[23]. Later, the stability, breakage, elastic properties of the liquid bridge were studied[24, 25]. The mechanics of a liquid bridge of the fiber-substrate system was recently analyzed by Qian and Gao[26]. They found that size reduction in liquid bridges can significantly enhance the wet adhesion.

Experiments show that the nature has evolved a variety of surface shapes, e.g. horseshoe, suction cup, and torus, etc., for wet adhesion[18, 20, 27–30]. In previous work, we studied the effects of different contact shapes on the adhesion force[31], focusing on flat, concave, convex and ring-like ones. The preliminary studies showed that a concave surface is more effective than the flat and convex ones, while the ring-like contact shape has advantages on a hydrophobic and rough surface. Bionic experimental studies[32, 33] also suggested that a concave surface can generate a much larger capillary force than a flat one. However, what the underlying mechanisms for the high capillary force of the concave surface are, and how to design an optimum concave surface are still elusive.

In this study, we will study the underlying physics of the robustness of the concave surface systematically by identifying the key factors that control the adhesion force, aiming to provide the guidelines for practical applications. The organization of the paper is as follows: In §II, we introduce the mechanical models for studying the wet adhesion of the concave tip. In §III, the mechanisms of the robustness are

discussed. A critical contact angle for the maximum strength and robustness of adhesion is derived. In §IV, a tentative design of the concave profile considering the chamfering size, deformation and bulking of the fiber tip is suggested. We briefly discussed the wet adhesion of multiple fibers via multiple liquid bridges in §V. Finally, conclusions are made in §VI.

II. MODEL

Figure 2 shows a fiber-liquid bridge-substrate system, where the fiber has a concave surface and the system is assumed axisymmetric. The insects or animals can make micro liquid bridges between their adhesion systems and the solid surface by secreting liquids. In the laboratory, the liquid bridge can be made by using the dosing needle. A liquid bridge can also form from the condensation of water vapor in the ambient air at appropriate relative humidity[34, 35]. To simplify the analysis and focus on the main physics of the problem, we make several assumptions as follows: a) the volume of liquid is conserved during the loading process; b) both the fiber and the substrate are rigid and do not deform, and the substrate is infinite in comparison with the liquid bridge; c) the loading process is quasi-static without considering the effect of the loading rate; d) the effect of gravity is assumed to be negligible as the typical size (diameter) of the fiber is smaller than the capillary length.

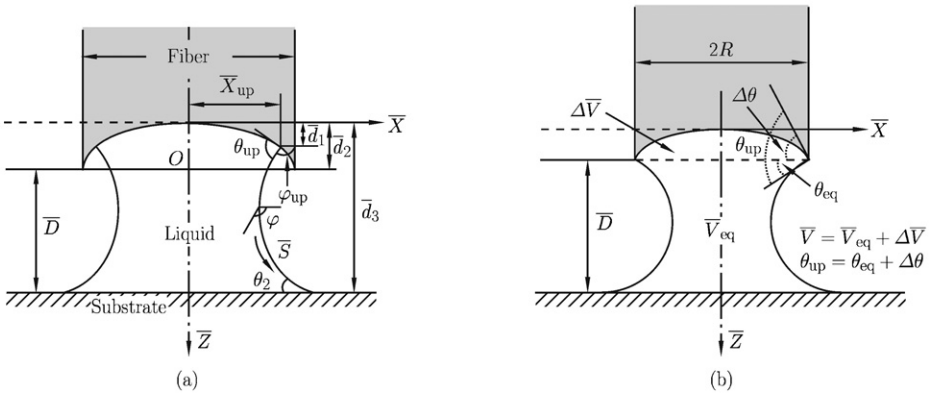

Fig. 2. The mechanical model of the fiber-liquid-substrate system. (a) Illustration of geometry of the system, including the liquid profile and its reference frame. (b) Illustration of the effective contact angle and the effective volume.

In the calculation of the adhesion force between the concave surface and the substrate, the core problem is to find the solution of the profile of the meniscus-like liquid bridge. Young-Laplace equation connects the pressure difference inside and outside the meniscus and the local liquid profile as,

$$\Delta P = \gamma \left(\frac{1}{R_1} + \frac{1}{R_2} \right) \tag{1}$$

where $1/R_1$ and $1/R_2$ denote the two local principal curvatures of the liquid profile, ΔP is the pressure difference which is constant within the meniscus due to the negligible gravity, and γ is interface energy between vapor and liquid. Interface energy γ is connected with the contact angles θ via the Young's equation,

$$\cos\theta = \frac{\gamma_{SV} - \gamma_{SL}}{\gamma} \tag{2}$$

where γ_{SV} and γ_{SL} are interface energy of solid-vapor and solid-liquid, respectively.

An ordinary differential equation can be derived from Young-Laplace equation,

$$\frac{\mathrm{d}\varphi}{\mathrm{d}s} = \frac{\Delta P}{\gamma} - \frac{\sin\varphi}{x}, \qquad \text{where} \quad \frac{\mathrm{d}x}{\mathrm{d}s} = \cos\varphi, \quad \frac{\mathrm{d}z}{\mathrm{d}s} = \sin\varphi \tag{3}$$

where x and z are the coordinates of the axisymmetric liquid bridge, φ is the angle between the local tangent of liquid surface and the horizontal axis, and s is the arc length of the liquid profile.

Introducing nondimensional units $\overline{X} = x/R$, $\overline{Z} = z/R$, $\overline{S} = s/R$, and $\overline{H} = (\Delta P \cdot R)/\gamma$, Eq.(3) can be rewritten as

$$\frac{\mathrm{d}\varphi}{\mathrm{d}\overline{S}} = \overline{H} - \frac{\sin\varphi}{\overline{X}}, \qquad \text{where} \quad \frac{\mathrm{d}\overline{X}}{\mathrm{d}\overline{S}} = \cos\varphi, \quad \frac{\mathrm{d}\overline{Z}}{\mathrm{d}\overline{S}} = \sin\varphi \tag{4}$$

The contact angle of liquid on the fiber surface is θ_1, and that on the substrate is θ_2. These two parameters are material constants, determined by the chemistry of the surfaces.

Previous studies had identified that there are two contact states between the fiber tip and the liquid during the pulling process of the liquid bridge:

a. Angle controlled state: The liquid meets the surfaces of the fiber within the circumference of the contact tip at the radius $\overline{X}_{\mathrm{up}}$ smaller than the fiber radius $\overline{R} = 1$; and $\theta_{\mathrm{up}} = \theta_1$. On the surface of the substrate, the liquid meets the solid always at the contact angle θ_2. Therefore, the boundary conditions for the angle controlled process are,

$$\varphi(\overline{Z} = \overline{d}_1) = \varphi_{\mathrm{up}} \quad \text{and} \quad \varphi(\overline{Z} = \overline{d}_3) = \theta_2 \tag{5a}$$

where $\overline{X}_{\mathrm{up}}$ is the radius of the contact line between the fiber and the liquid assuming it is a circle (see Fig.2(a)) which can be calculated according to $\overline{D}$, where $\overline{D}$ is the separated distance between the fiber tip and the substrate.

b. Radius controlled state: The liquid periphery is pinned at the circumference of the fiber tip, and the liquid meets the surfaces of the fiber tip at the angle θ_{up} different from their material contact angle θ_1; On the surface of the substrate, the liquid meets the solid always at the contact angle θ_2. Therefore, the boundary conditions for the radius controlled process are,

$$\overline{X}(\overline{Z} = \overline{d}_2) = 1 \quad \text{and} \quad \varphi(\overline{Z} = \overline{d}_3) = \theta_2 \tag{5b}$$

where φ_{up} can be calculated according to the separation $\overline{D}$. And $\overline{X}_{\mathrm{up}} = 1$.

The liquid volume can be calculated by the following integral,

$$\overline{V} = \int_{\overline{\Omega}} \pi \cdot \overline{X}^2 \mathrm{d}\overline{Z} \tag{6}$$

According to the expression of the adhesion force

$$F = -\pi r^2 \Delta P + 2\pi r \gamma \sin\theta \tag{7a}$$

the normalized adhesion force can be calculated as follows,

$$\eta = -\overline{X}_{\mathrm{up}}^2 \overline{H} + 2\overline{X}_{\mathrm{up}} \sin\varphi_{\mathrm{up}} \tag{7b}$$

In order to show the advantage of the concave surface in comparison with the flat one, we would like to introduce the concepts of the effective contact angle and effective liquid volume for the convenience of the comparison between the concave one and the flat one:

Definition 1: The effective contact angle θ_{eq} is defined as the angle at the triple point between the tangent line of the liquid profile and the horizontal line (two dimensional), as shown in Fig.2(b). We can see that, for the concave tip, $\theta_{\mathrm{up}} = \theta_{\mathrm{eq}} + \Delta\theta$, where $\Delta\theta$ is the angle between the tangent line of the concave profile and the horizontal line. The concept of effective contact angle is applicable at both radius controlled and angle controlled states.

Definition 2: The effective liquid volume $\overline{V}_{\mathrm{eq}}$ is defined as the volume of liquid under the horizontal plane passing the outer edge of the concave surface, as shown in Fig.2(b). The total volume of the liquid bridge under the concave surface is $\overline{V} = \overline{V}_{\mathrm{eq}} + \Delta\overline{V}$ and $\overline{V}_{\mathrm{eq}} < \overline{V}$, where $\Delta\overline{V}$ is the volume between the horizontal plane and the concave surface. Therefore, for flat tips, the effective liquid volume equals its total volume $\overline{V}$. The concept of effective volume is applicable at only Radius controlled state.

III. RESULTS AND DISCUSSION

3.1. Results

Figure 3 shows a typical deformation process of the liquid bridge between the concave surface and substrate under the pulling force, exhibiting two state transitions during the whole detaching process. The first transition happens from the radius controlled state to the angle controlled one, and the second transition from the angle controlled state to the radius controlled one. We previously showed that the two transitions also similarly happen for the flat surface and that transition I is a critical point because it determines how large the maximum adhesion force the fiber can achieve. The later the transition I happens, the larger the adhesion force is. Here we show that the concave surface can effectively delay transition I.

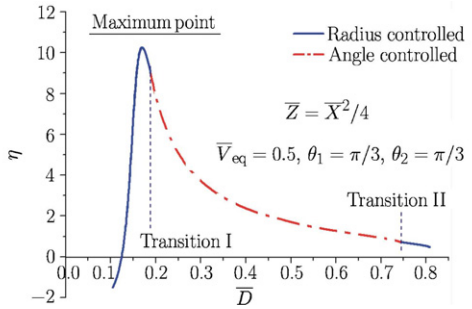

Fig. 3 A typical loading process of the fiber-liquid-substrate system with a concave tip which shows the evolution of the profile of the liquid as the contact state between the fiber and liquid changes from radius controlled to angle controlled, and then comes back to radius controlled state before the liquid bridge collapses.

We find that the concave surface can induce a larger detaching force (i.e. maximum adhesion force) than the flat one under the condition of the same effective liquid volume. The maximum force changing with the fiber-liquid contact angle is of particular interest. Figure 4 shows the relationship of the maximum force versus the contact angle θ_1 for different contact surfaces: two concave surfaces, characterized by the profiles, $\overline{Z} = \overline{X}^{10}/4$ and $\overline{Z} = \overline{X}^2/4$, and a flat one. We can see that the maximum force starts to decrease at $\theta_1 = 15°$ for the flat tip, in contrast, the maximum force for the concave tip $\overline{Z} = \overline{X}^2/4$ does not decrease until the contact angle θ_1 is increased to as larger as 45°, implying the adhesive system becoming less sensitive to the contact angle θ_1. This can be called the 'robustness' of the contact surface on the variation of material chemistry. When we further enlarge the curvature of the concave surface to, e.g. $\overline{Z} = \overline{X}^{10}/4$, the maximum force will not decrease until the contact angle is increased to $\theta_1 = 90°$, and the maximum force decreases only a little at a contact angle $\theta_1 = 120°$, exhibiting stronger robustness of adhesion. We further calculate the evolution of the maximum force with the contact angle θ_1 at different θ_2 for a concave surface $\overline{Z} = \overline{X}^2/4$ (see Fig.5), which shows the robustness of the concave surface exists at various contact angles θ_2. This property is of great advantage for insects to adhere on the surface with different chemistry by choosing a concave tip.

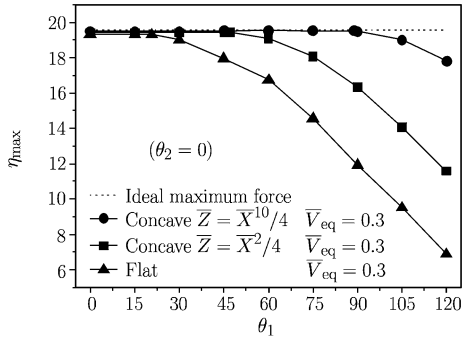

Fig. 4. The relationship between the maximum adhesion force (detaching force) and the contact angle θ_1 for different contact shapes: the concave ones $\overline{Z} = \overline{X}^{10}/4$ and $\overline{Z} = \overline{X}^2/4$, and the flat one. It shows that the concave shape make the detaching force more insensitive to the change of contact angle θ_1.

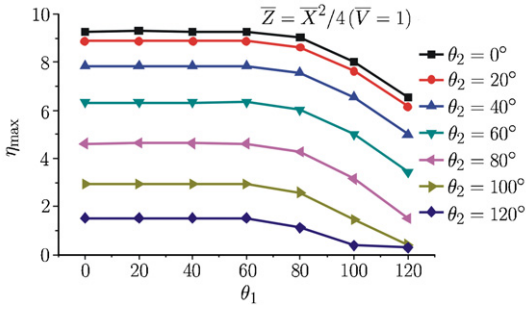

Fig. 5. The evolution of the maximum adhesion force (detaching force) with the contact angle θ_1 at various θ_2 with concave profile $\overline{Z} = \overline{X}^2/4$, showing the robustness of the concave surface at different contact angle θ_2.

3.2. Critical Angle for Robustness

Why does the concave surface enhance the adhesion force and make it insensitive to the variation of the contact angle? We find that the concave surface can transfer the large real contact angle to a small effective contact angle, effectively retarding the radius-to-angle controlled transition (transition I), and therefore enhances the adhesion force. Figure 4 shows that the higher the degree of the concavity of the surface, the stronger the retarding effect is. When the effective contact angle $\theta_{\rm eq}$ is smaller than a critical angle θ^* in the system (see Fig.4), transition I will happen after the adhesion force reaches the critical point for the ideal maximum force, i.e. the adhesive force achieves the ideal maximum force. In contrast, if transition I happens before the point for the ideal maximum force, the detaching force will not achieve the maximum value. In order to enhance the adhesive force, $\theta_{\rm eq}$ should be as small as possible to delay transition I and preserve the robustness of the system.

Figure 5 shows that $\theta^*_{\rm eq}$ is almost independent of θ_2 at a specific liquid volume $\overline{V}_{\rm eq} < 1$. To derive an analytical solution of $\theta^*_{\rm eq}$, we assume $\theta_2 = \pi$ under which the profile of the liquid bridge is a sphere (Figs.6(a) and (b)) when its detaching force reaches its maximum value (being equal to zero). The profile can be described as

$$\overline{X}(\varphi) = \frac{2\sin\varphi}{\overline{H}}, \quad \overline{Z}(\varphi) = -\frac{2\cos\varphi}{\overline{H}} + C_0 \tag{8}$$

The nondimensional pressure is

$$\overline{H} = 2\sin\theta^*_{\rm eq} \tag{9}$$

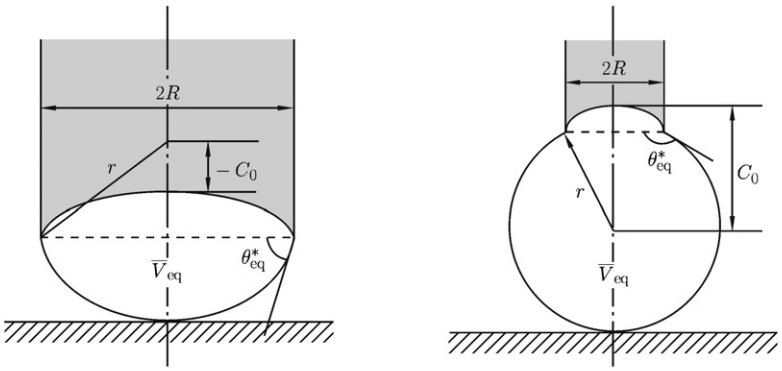

Fig. 6. Illustration of the liquid profile at its maximum adhesion force (detaching force) at $\theta_2 = \pi$.

and the liquid volume can be obtained as,

$$\overline{V}_{\rm eq} = \int_{\overline{\Omega}} \pi \cdot \overline{X}^2 {\rm d}\overline{Z} = \frac{\pi \sin\theta^*_{\rm eq}(\cos\theta^*_{\rm eq} + 2)}{3(\cos\theta^*_{\rm eq} + 1)^2} \tag{10}$$

Then the expression of $\theta^*_{\rm eq}$ can be obtained in terms of the nondimensional liquid volume,

$$\theta^*_{\rm eq} = \arccos\left\{ -1 + \frac{1}{\left[(1+\overline{Y})^2 + \sqrt{\overline{Y}(1+\overline{Y})^3}\right]^{1/3}} + \frac{\left[(1+\overline{Y})^2 + \sqrt{\overline{Y}(1+\overline{Y})^3}\right]^{1/3}}{1+\overline{Y}} \right\} \tag{11}$$

where $\overline{Y} = (\frac{3}{\pi}\overline{V}_{\rm eq})^2$. Figure 7 shows that $\theta^*_{\rm eq}$ increases with the increase of the nondimensional liquid volume. For comparison, we numerically calculate the relationship of $\theta^*_{\rm eq}$ versus the nondimensional liquid volume for another extreme condition, $\theta_2 0$ (see Fig.7). We find that the difference in $\theta^*_{\rm eq}$ for $\theta_2 = 0$ and $\theta_2 = \pi$ at different liquid volumes is small, particularly when $\overline{V} < 1$ which often happens in biological adhesive systems (which can not have so much liquid). In the following, we rewrite $\theta^*_{\rm eq}$ as $\theta^*(\overline{V}_{\rm eq})$ to denote that it is mainly changed with the non-dimensional liquid volume.

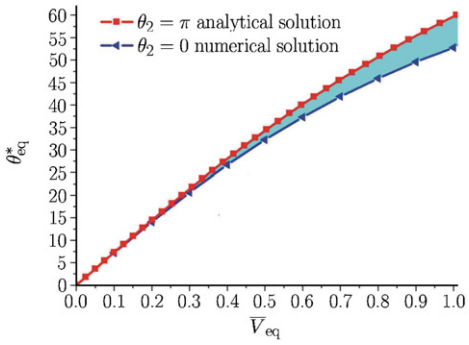

Fig. 7. The relationship of θ^*_{eq} versus $\overline{V}_{eq}$. The lower curve is the result for $\theta_2 = 0$, while the upper curve is the analytical result for $\theta_2 = \pi$. When $0 \le \theta_2 \le \pi$, the value of θ^*_{eq} will adopt a value in the inter-region between the two curves.

IV. TENTATIVE DESIGN FOR CONCAVE PROFILE

According to our previous studies and discussions, the concave surface can effectively enhance the wet adhesion. Here we discuss how to design a concave surface in practical applications. In addition to the design of the profile of the surface, one should also consider other key factors, such as the effect of the chamfering at the circumference of contact tips, and mechanical properties of the fiber, including static deformation, elastic instability, etc. An optimum concave surface shall satisfy the following requirements: a) The adhesive force can reach the ideal maximum force; b) The deformation of the fiber tip should be so small that that it does not influence the profile of the liquid bridge and the adhesive force; c) The negative pressure produced by the liquid does not cause buckling of the concave tip.

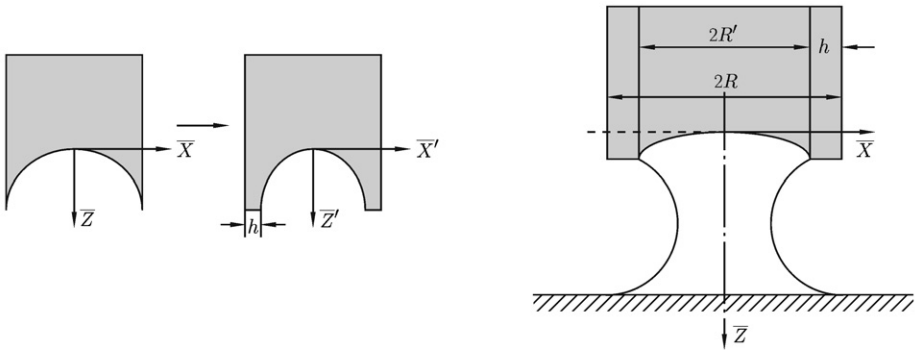

Fig. 8. The mechanical model of the contact surface with chamfering.

To explain how to design an optimum tip, we describe the profile of the contact surface in the coordinates shown in Fig.8 with the following function,

$$\overline{Z} = g(\overline{X}) \tag{12}$$

where

$$g(0) = 0 \quad \text{and} \quad g(\overline{X}) = g(-\overline{X}) \tag{13}$$

from which the extra-volume $\Delta\overline{V}$ and the effective contact angle θ_{eq} can be calculated as

$$\Delta\overline{V} = \int_0^1 \pi \cdot \overline{X}^2 \cdot g'(\overline{X}) \mathrm{d}\overline{X} \tag{14a}$$

$$\theta_{eq} = \theta_1 - \Delta\theta = \theta_1 - \arctan[g'(1)] \tag{14b}$$

If we choose the power function to describe the profile of the concave surface, i.e., $g(\overline{X}) = \overline{X}^n/k$, the extra-volume and the effective contact angle are $\Delta\overline{V} = n\pi/[k(n+2)]$ and $\Delta\theta = \arctan(n/k)$,

respectively. In order to satisfy the following criterion for the robustness of the wet adhesion,

$$\theta_{\rm eq} < \theta^*(\bar{V}_{\rm eq}) \tag{15a}$$

one should enlarge $\Delta\theta$ to reduce the effective contact angle $\theta_{\rm eq}$. We denote $t = n/k = g'(1)$, then the extra-value is $\Delta\overline{V} = t\pi/(kt+2)$. We can see that t controls the extra-angle $\Delta\theta$ and $\Delta\overline{V}$, and $\Delta\overline{V}$ decreases with the increasing of variable k. According to Eq.(15a), an optimum concave tip should satisfy,

$$t > \tan[\theta_1 - \theta^*(\overline{V}_{\rm eq})] \tag{15b}$$

Above analyses show that the contact surface should be as more concave as possible in order to enhance the adhesive force and preserve the robustness of the adhesion system. However, the slope of the tip t can not be too large because the real material may not be stiff enough to keep the geometrical shape under the external load. Therefore, in practice, the fiber tip can not be absolute sharp-angled, instead there is chamfering on the fiber tip, as shown in Fig.8(b). In this study, we choose a flat chamfering. One can also choose other chamfering geometries, such as semi-circle like with radius r'. However, the flat chamfering allows us to make comparison between the tip with chamfering and that without chamfering more rigorously, because a non-flat chamfering will cause the definition of the effective volume inconsistent between the tip with chamfering and that without chamfering.

In order to consider the influence of the chamfering on the adhesion force, we first define the effective radius of the fiber is $R' = R - h$ because of the chamfering as shown in Fig.8(b). Then the relationship of the adhesive force and the liquid volume will be,

$$\eta' = \eta'(\overline{V}', \theta_1, \theta_2, \overline{D}) \tag{16}$$

where

$$\overline{V}' = \frac{R^3}{R'^3}\overline{V} \tag{17}$$

and

$$\eta = \eta'\frac{R'}{R} \tag{18}$$

The symbol $'$ indicates the variable normalized by R'. We can calculate the normalized liquid volume $\overline{V}'$ from Eq.(17), and obtain the adhesive force η' from Eq.(16), then the normalized adhesive force η from Eq.(18).

Figure 9 shows the force-distance curves for different sizes of chamfering. There are two peaks on the curves when the chamfering is larger than zero. While the first peak does not change with the variation of the size of chamfering, the second peak decreases with the increase of the chamfering size. When the chamfering size is small, the second peak is higher than the first peak, therefore concave surfaces

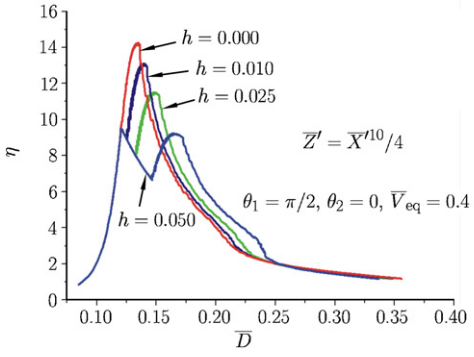

Fig. 9. The force-separation curves for various concave surfaces with and without chamfering. For the surface with chamfering, each curve has two peaks. While the position and value of the first peak are same for different curves, the second peaks decrease with the increase of the chamfering size.

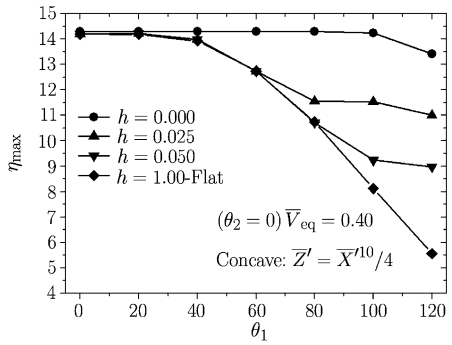

Fig. 10. The relationship between the maximum adhesion force (detaching force) and the contact angle θ_1 for the flat tip and the concave surfaces with different chamferings, showing the effect of chamfering size on the maximum adhesion force.

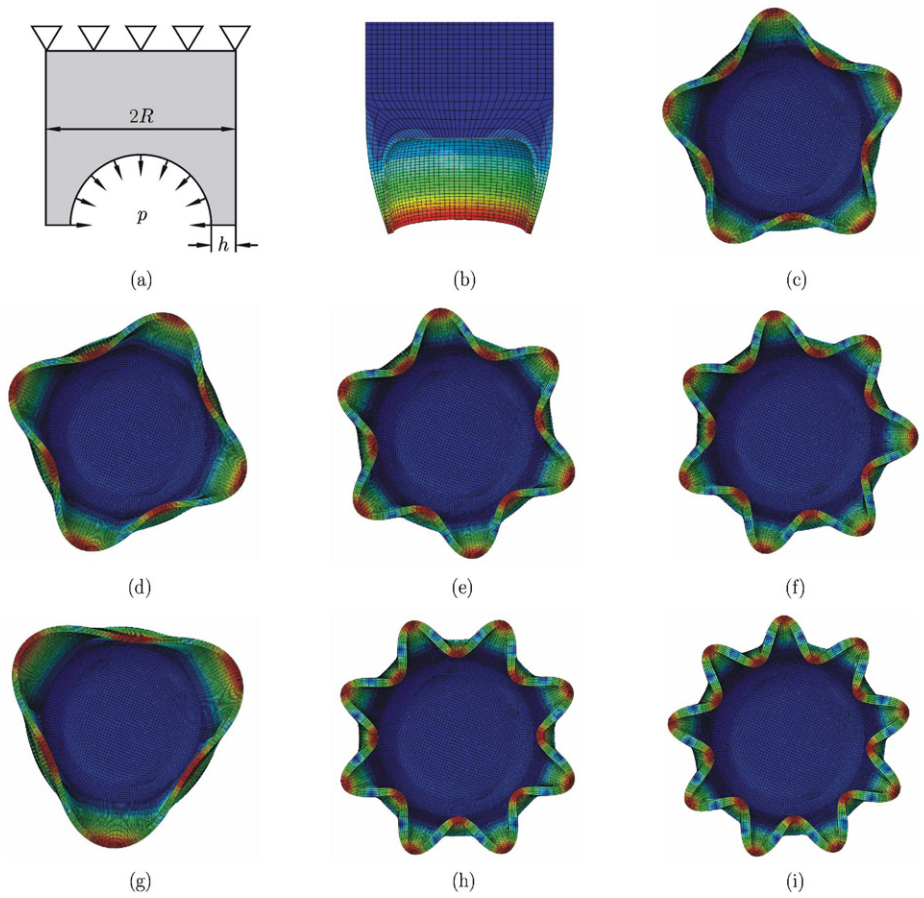

Fig. 11. The FEM model for analysis of the static deformation and elastic instability of the concave tip. (a) FEM model showing the constraint and loading applied on the system. (b) the static deformation; (c)-(i) the lowest 7 buckling modes.

can enhance the wet adhesion. However, the concave surface will not have effect on the adhesion if the chamfering size is so large that the second peak is lower than the first peak. In order to enhance the adhesive force, the size of the chamfering shall be as small as possible. Figure 10 depicts the influence of the chamfering size on the adhesion force at different contact angles θ_1, showing the robustness of the concave tip of different chamfering sizes. The smaller the chamfering size, the higher the adhesion force at which the robustness can be achieved.

In previous analyses, the fiber was considered as rigid. However, in practical design, we should consider the deformation and the elastic stability of the structure due to the negative pressure acted by the liquid. Figure 11(a) shows the mechanical model in our analyses, where the profile of the contact surface is described by $\overline{Z}' = \overline{X}'^n/k$ and the size of the chamfering is h. The fiber is fixed at its upper terminal, and is loaded on the contact surface by a pressure p coming from the inner negative pressure of the liquid bridge. The negative pressure applied is -1.5 MPa which is the maximum negative pressure that the liquid bridge can have beyond which the liquid will be gasified. And $h = 0.05$.

The normalized deformation of the fiber tip for different profiles (i.e. for various n, k values) is shown in Table 1, which shows that the deformation increases with the concavity of the profile ($n \uparrow$ and $k \downarrow$). Since large deformation will affect the adhesion force, there shall be an optimum concavity for the maximum adhesion force for a specific h. The elastic stability of the fiber tip under negative pressure is also an important problem. If the wall of the fiber tip is too thin because of high concavity of its profile, the tip will buckle because of the negative pressure. The critical pressure for buckling of the concave tips of different concavity is shown in Table 2. The first seven buckle modes for $n = 10$ and $k = 1$ are shown in Figs.11(c)$\sim$11(i) and the critical pressure is 1.59 MPa larger than the limited pressure in liquid. We see that the water pressure normally can not cause the fiber tip to buckle.

Table 1. **The normalized deformation of concave tip at different values of n and k.**

$\bar{u}_{\max}$	$n=10$	$n=8$	$n=6$	$n=4$	$n=2$
$k=1$	2.45×10^{-2}	2.35×10^{-2}	2.28×10^{-2}	1.74×10^{-2}	9.70×10^{-3}
$k=2$	1.63×10^{-2}	1.38×10^{-2}	1.04×10^{-2}	7.04×10^{-3}	3.37×10^{-3}

Table 2. **The normalized deformation of concave tip at different values of n and k.**

$p_{\rm cri}$	$n=10$	$n=8$	$n=6$	$n=4$	$n=2$
$k=1$	1.65 MPa	2.05 MPa	2.98 MPa	5.62 MPa	11.2 MPa
$k=2$	7.0 MPa	10.5 MPa	16.2 MPa	35.9 MPa	66.5 MPa

V. MULTIPLE LIQUID BRIDGES

In the preceding analyses, we studied the wet adhesion of a single fiber. Now we extend our analysis to multiple fibers to mimic the adhesion of a seta structure with many spatulae. For the analysis of multiple-fiber systems, we adopt a two dimensional model for simplicity without losing the main physics of the problem (see Fig.12). The conclusion of the results can generally be extended to the 3D system. In a 2D system, Eq.(4) degenerates to

$$\frac{\mathrm{d}\varphi}{\mathrm{d}\overline{S}}=\overline{H},\qquad \text{where}\quad \frac{\mathrm{d}\overline{X}}{\mathrm{d}\overline{S}}=\cos\varphi,\quad \frac{\mathrm{d}\overline{Z}}{\mathrm{d}\overline{S}}=\sin\varphi \tag{19}$$

and its analytical solution is

$$\overline{X}(\varphi)=\frac{\sin(\varphi)}{\overline{H}}+C_1,\quad \overline{Z}(\varphi)=-\frac{\cos(\varphi)}{\overline{H}}+C_2 \tag{20}$$

which shows that the liquid profile is a circular arc. Point (C_1,C_2) is the centre of the circle, and $1/\bar{H}$ is the radius. When the total volume of the liquid is small so that each fiber has its own liquid bridge as shown in Fig.12(a), the adhesive stress can be expressed as

$$\sigma_a=\eta_a\frac{\gamma}{\lambda} \tag{21}$$

where λ is the distance between two neighboring fibers (see Fig.12(a)), and

$$\eta_a=-\overline{X}_{\rm up}\overline{H}+\sin\varphi_{\rm up} \tag{22}$$

Equation (21) shows the adhesion force per unit area, i.e. adhesion stress, inversely increases with λ. If the total contact area is kept constant, the total adhesion force will rapidly increase when the fiber size and distance are reduced, i.e., having small hairs in high density. If the liquid is overabundant, the

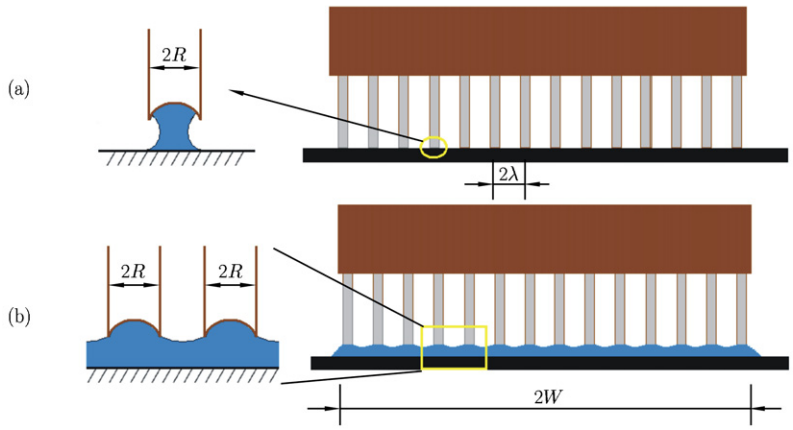

Fig. 12. The mechanical model for multiple liquid bridges at different liquid volume. (a) at small liquid volume; (b) at large liquid volume.

liquid bridges will coalesce into one big liquid bridge as shown in Fig.12(b), and the adhesion stress becomes,

$$\sigma_b = \eta_b \frac{\gamma}{W} \tag{23}$$

where W is the size of the seta, and $W \gg \lambda$. The coefficient η_b is the function of the liquid volume. At the very beginning of coalescence, η_b is in the same order of magnitude as $\eta_a W/\lambda$, therefore, $\sigma_b \approx \sigma_a$. However, as the volume of liquid is further increased, the adhesive stress will fall rapidly, and $\sigma_b \ll \sigma_a$ at large liquid volumes.

VI. CONCLUSIONS

This paper presents a theoretical study of mechanics of wet adhesion of fibers with a substrate via liquid bridges by modeling the mechanics of materials at small scales, inspired by the exquisite structures of biological surfaces. We found that the contact shape plays an important role in the wet adhesion and the concave shape can significantly enhance the adhesion and make the adhesion strength insensitive to chemistry of materials. The underlying physics of the robustness of wet adhesion of concave surfaces was studied by analyzing the contact states of surfaces during the loading process. The effective contact angle of the concave surface is identified as a critical parameter controlling the mechanics of the wet adhesion. When the effective contact angle is smaller than a critical value, the surface will always achieve the maximum adhesion strength and robustness. An analytical expression for the critical contact angle was derived, which is critical for the profile design of concave surfaces. A design method of concave profile considering the effect of the chamfering size, static deformation and buckling properties of contact tips was suggested. We showed that biological systems use the material and structure simultaneously at the small scale to achieve superior properties. This study may provide guidelines for the design of bioinspired micro- and nano-devices , such as in MEMS and NEMS, for manipulating microscopic objects. It is also aimed to raise more research interests in this fertile and challenging area.

References

[1] Walker,G., Adhesion to smooth surfaces by insects — A review. *International Journal of Adhesion and Adhesives*, 1993, 13: 3-7.

[2] Barnes,W.J.P., Dynamic adhesion in animals: mechanisms and biomimetic implications. *Journal of Comparative Physiology A,* 2006, 192: 1165-1168.

[3] Scherge,M. and Gorb,S., Biological Micro- and Nanotribilogy: Nature's Solutions. Heidelberg: Springer Verlag, 2001.

[4] Jiao,Y.K., Gorb,S. and Scherge,M., Adhesion measured on the attachment pads of tettigonia viridissima (Orthoptera, Insecta). *Journal of Experimental Biology,* 2000, 203: 1887-1895.

[5] Gorb,S., Gorb,E. and Kastner,V., Scale effects on the attachment pads and friction forces in syrphid flies. *Journal of Experimental Biology,* 2001, 204: 1421-1431.

[6] Autumn,K., Peattie, A.M., Mechanisms of adhesion in geckos. *Integrative and Comparative Biology,* 2002, 42: 1081-1090.

[7] Kesel,A.B., Martin,A. and Seidl,T., Getting a grip on spider attachment: an AFM approach to microstructure adhesion in arthropods. *Smart Materials & Structures,* 2004, 13: 512-518.

[8] Autumn,K., Sitti,M., Liang,Y.C.A., Peattie,A.M., Hansen,W.R., Sponberg,S., Kenny,T.W., Fearing,R., Israelachvili,J.N. and Full,R.J., Evidence for van der Waals adhesion in gecko setae. *Proceedings of the National Academy of Sciences of the United States of America,* 2002, 99: 12252-12256.

[9] Arzt,E., Gorb,S., Spolenak,R., From micro to nano contacts in biological attachment devices. *Proceedings of the National Academy of Sciences of the United States of America,* 2003, 100: 10603-10606.

[10] Gao,H.J., Wang,X., Yao,H.M., Gorb,S., Arzt,E., Mechanics of hierarchical adhesion structures of geckos. *Mechanics of Materials,* 2005, 37: 275-285.

[11] Buehler,M.J., Yao,H.M., Gao,H.J., Ji,B.H., Cracking and adhesion at small scales: atomistic and continuum studies of flaw tolerant nanostructures. *Modelling and Simulation in Materials Science and Engineering,* 2006, 14: 799-816.

[12] Buehler,M.J., Yao,H.M., Ji,B.H., Gao,H.J., Atomistic and continuum studies of flaw tolerant nanostructures in biological systems. *Mechanical Properties of Bioinspired and Biological Materials,* 2005, 844: 207-212.

[13] Cao,H.J., Ji,B.H., Buehler,M.J., Yao,H.M., Flaw tolerant nanostructures of biological materials. *Mechanics of the 21st Century,* 2005, 131-138.

[14] Gao,H., Ji,B., Buehler,M.J., Yao,H., Flaw tolerant bulk and surface nanostructures of biological systems. *Mechanics and Chemistry of Biosystems,* 2004, 1: 37-52.
[15] Gao,H., Ji,B., Jager,I.L., Arzt,E., Fratzl,P., Materials become insensitive to flaws at nanoscale: Lessons from nature. *Proceedings of the National Academy of Sciences of the United States of America,* 2003, 100: 5597-5600.
[16] Ji,B., Gao,H., Mechanical properties of nanostructure of biological materials. *Journal of the Mechanics and Physics of Solids,* 2004, 52: 1963-1990.
[17] Ji,B.H., A study of the interface strength between protein and mineral in biological materials. *Journal of Biomechanics,* 2008, 41: 259-266.
[18] Spolenak,R., Gorb,S., Gao,H.J., Arzt,E., Effects of contact shape on the scaling of biological attachments. *Proceedings of the Royal Society of London Series A — Mathematical Physical and Engineering Sciences,* 2005, 461: 305-319.
[19] Federle, W., Riehle, M., Curtis, A. S. G., Full, R. J., An integrative study of insect adhesion: Mechanics and wet adhesion of pretarsal pads in ants. *Integrative and Comparative Biology,* 2002, 42: 1100-1106.
[20] Gao,H.J., Yao,H.M., Shape insensitive optimal adhesion of nanoscale fibrillar structures. *Proceedings of the National Academy of Sciences of the United States of America,* 2004, 101: 7851-7856.
[21] Huber,G., Mantz,H., Spolenak,R., Mecke,K., Jacobs,K., Gorb,S.N., Arzt,E., Evidence for capillarity contributions to gecko adhesion from single spatula nanomechanical measurements. *Proceedings of the National Academy of Sciences of the United States of America,* 2005, 102: 16293-16296.
[22] Sun,W.X., Neuzil,P., Kustandi,T.S., Oh,S., Samper,V.D., The nature of the gecko lizard adhesive force. *Biophysical Journal,* 2005, 89: L14-L17.
[23] Orr.,F.M., Scriven.L.E., Pendular rings between solids: meniscus properties and capillary force. *Journal of Fluid Mechanics,* 1975, 67: 723-742.
[24] Choe,H., Hong,M.H., Seo,Y., Lee,K., Kim,G., Cho,Y., Ihm,J., Jhe,W., Formation, manipulation, and elasticity measurement of a nanometric column of water molecules. *Physical Review Letters,* 2005, 95.
[25] Padday,J.F., Petre,G., Rusu,C.G., Gamero,J., Wozniak,G., The shape, stability and breakage of pendant liquid bridges. *Journal of Fuid Mechanics,* 1997, 352: 177-204.
[26] Qian,J., Gao,H.J., Scaling effects of wet adhesion in biological attachment systems. *Acta Biomaterialia,* 2006, 2: 51-58.
[27] Gorb,S., Jiao,Y.K., Scherge,M., Ultrastructural architecture and mechanical properties of attachment pads in Tettigonia viridissima (Orthoptera Tettigoniidae). *Journal of Comparative Physiology A — Neuroethology Sensory Neural and Behavioral Physiology,* 2000, 186: 821-831.
[28] Scherge,M., Gorb,S.N., Using biological principles to design MEMS. *Journal of Micromechanics and Microengineering,* 2000, 10: 359-364.
[29] Federle,W., Brainerd,E.L., McMahon,T.A., Holldobler,B., Biomechanics of the movable pretarsal adhesive organ in ants and bees. *Proceedings of the National Academy of Sciences of the United States of America,* 2001, 98: 6215-6220.
[30] Langer,M.G., Ruppersberg,J.P., Gorb,S., Adhesion forces measured at the level of a terminal plate of the fly's seta. *Proceedings of the Royal Society of London Series B-Biological Sciences,* 2004, 271: 2209-2215.
[31] Su,Y.W., Ji,B.H., Huang,Y.G., Hwang,K.H., Effects of contact shape on biological wet adhesion. *Jounal of Materials Science,* 2007, 42: 8885-8893.
[32] Obata, K. J., Motokado, T., Saito, S., Takahashi, K., A scheme for micro-manipulation based on capillary force. *Journal of Fluid Mechanics,* 2004, 498: 113-121.
[33] Saito,S., Motokado,T., Obata,K.J., Takahashi,K., Capillary force with a concave probe-tip for micromanipulation. *Applied Physics Letters,* 2005, 87: 234103.
[34] Butt,H.J., Kappl,M., Normal capillary forces. *Advances in Colloid and Interface Science,* 2009, 146: 48-60.
[35] Wei,Z., Zhao,Y.P., Growth of liquid bridge in AFM. *Journal of Physics D — Applied Physics*, 2007, 40: 4368-4375.